Development of Adiabatic Shear Bands in Annealed 316L Stainless Steel: Part II. TEM Studies of the Evolution of Microstructure during Deformation Localization

Q. XUE and G.T. GRAY, III

The evolution of adiabatic shear localization in an annealed AISI 316L stainless steel has been investigated and was reported in Part I of this paper (*Met. Trans. A*, 2006, Vol. 37A, pp. 2435-446). In the present research (Part II), a comprehensive transmission electron microscopy (TEM) examination was conducted on the microstructural evolution of shear localization in this material at different loading stages. The TEM results indicate that elongated subgrain laths and an avalanche of dislocation cells are the major characteristics in an initiated band. Development of the substructures within shear bands is controlled by dynamic recovery and continuous dynamic recrystallization. The core of shear bands was found to consist of fine equiaxed subgrains. Well-developed shear bands are filled with a mixture of equiaxed, rectangular, and elongated subgrains. The equiaxed subgrains, with a typical size less than 100 nm, are postulated to result from either the breakdown and splitting of subgrain laths or the reconstruction of subcells.

I. INTRODUCTION

ADIABATIC shear localization (shear band) is an important damage/failure mode of materials during high-strain-rate deformation. This failure mode is characterized as an unstable behavior of deformation to form a band-like localized deformation region in a nearly adiabatic process.[1,2] Although thermal softening in a shear band can finally lead to a rapid failure and makes the material lose its local load-bearing capacity, unlike cracking, the material inside a shear band may still maintain a weak continuity. Once a shear band forms, thermal softening dominates the subsequent development of shear bands. Severe plastic deformation within a shear band at high strain rates leads to a drastic rise of temperature, even up to the melting point of the material. The microstructure within shear bands observed in postmortem observations provides ample information of this failure process.[3] However, the material inside shear bands possesses complicated substructures that experience multiple transitions of deformation modes, combined stress and temperature history, and rapid quenching after the deformation. The analysis and decoding of the combined effects on the substructures is quite difficult but is critical to understand the process and mechanisms of shear localization.

The propensity of materials to adiabatic shear localization has been extensively studied since this phenomenon was reported.[1–12] A broad range of materials, including metals and their alloys, polymers, ceramics, and composites, have been examined under different dynamic loading processes.[1,2,7,8,9,13,14] The development of substructures within shear bands received a great attention to determine effects of material parameters on shear band initiation, morphology, and mechanisms to generate such substructures.[1,3,7–11] Many early documents attribute the white etching inside shear bands in steels to a phase transformation product. A plausible explanation is that at the high temperatures generated inside shear bands, steels austenize and subsequently quench into martensites through a phase transformation ($\gamma \rightarrow \alpha'$).[3] Some recent TEM results have suggested that the fine substructure may not in fact come from this transformation but instead from recrystallization.[15] The residual products within shear bands were found to have formed *via* different mechanisms, related to the locally high temperatures and high shear stresses. The potential mechanisms controlling the residual substructures within shear bands include dynamic and/or static recovery, dynamic and/or static recrystallization, and phase transformation. Some researchers have also reported amorphous regions within shear bands.[16] Although metallurgists have invested a great deal of effort into exploring the products of shear bands in the past half-century, there remains very limited knowledge of the systematic evolution of microstructure during the nucleation and growth stages of shear localization.

The substructures within shear bands have been widely studied using TEM in different materials, including brass (70-30 Cu-Zn),[17] Al alloys,[18] alloy steels in different heat treatment conditions,[19–22] and commercially pure (CP) Ti and Ti alloys.[23–25] TEM examinations have revealed the detailed substructures within shear bands and have provided extensive information for understanding the process of adiabatic localization. However, previous TEM examinations have mainly explored the residual substructure within shear bands at specific loading stages. The morphology of the residual substructures inside shear bands has been reported in regard to various random aspects. Because adiabatic shear bands develop at extremely high strain rates (up to $10^5 \sim 10^6$ s^{-1}), it is very hard to capture a shear band at a designated stage of its formation. There is also a lack of well-controlled shear conditions required to ''freeze'' shear bands at different evolving stages. Previous studies have indicated that hot-rolled steels and annealed steels, such as stainless steels, do not readily form adiabatic shear bands.[7,13] How shear localization initiates and develops

Q. XUE, Research Associate, and G.T. GRAY, III, Technical Staff Member, are with the Division of Materials Science and Technology, Los Alamos National Laboratory, Los Alamos, NM 87545. Contact e-mail: qxue@lanl.gov

Manuscript submitted December 1, 2005.

in such a material that is not susceptible to unstable deformation is important to the understanding of the dominant mechanisms controlling shear localization.

Part I of this paper (*Met. Trans. A*, 2006, Vol. 37A, pp. 2435-446) reported a study correlating the evolving microstructure to the corresponding mechanical response during shear localization in an annealed (as-received) AISI 316L stainless steel. Postmortem observations of the shear band microstructure were performed and correlated to the mechanical response. The complete progression of shear band evolution from formation through final development was examined. In the present paper, a comprehensive microstructural examination of shear band evolution using TEM is presented. The microstructures within the shear sections of specimens loaded to a series of critical points of the shear deformation were extensively investigated. The mechanisms that control the resultant substructures within shear bands are proposed and discussed in accordance with the observed results.

II. EXPERIMENTAL PROCEDURES

The details of the tested material (316L SS) and the forced shear experiments were described in Part I. A series of hat-shaped specimens loaded to different shear displacements were correlated to several stages of shear localization. The sheared sections of hat-shaped specimens were examined using both optical microscopy (OM) and TEM. The results reported in this paper emphasize the TEM examination, in which the resolution is about 100 times larger than the OM observations detailed in Part I. The term ''microstructure'' as used in Part I and in Part II involves different length scales. The postmortem examinations of these samples exhibit the microstructural evolution of adiabatic shear localization in these very short loading durations.

The TEM samples were cut from both the untested 316L SS plate and the tested hat-shaped specimens. Hat-shaped specimens were bisected along the loading axis direction and a 200-μm-thick sheet was cut parallel to the bisected surface using a low-speed diamond saw. The shear section containing the localized deformation is sandwiched between the two notched tips at both the punch-in and punch-out ends of the hat-shaped specimen. The residual length of the sheared section retained is 0.2~0.5 mm after the tests. These sheet samples were mechanically thinned and polished to a thinner foil. Three-millimeter disks were carefully cut to align the shear band paths exactly through the center of the disks. The schematic procedure of the sample preparation is shown in Figure 1. Dimpling was carried out on a Gatan dimpler to more precisely thin the TEM foil exactly within the shear band region. Ion milling was performed on a Gatan Precision Ion Polishing system (PIPs) to ensure that the perforation was accurately located on the paths of the shear bands. A Philips CM30 TEM at 300 kV was used to examine the substructure of the materials in both the as-received and localized areas.

III. RESULTS

The substructure of the as-received 316L SS was examined and analyzed. The microstructure was found to consist of a low dislocation density and a few scattered stacking faults (Figure 2). 316L stainless steel is a typical face-center-cubic (FCC) metal with low stacking fault energy. Slip primarily occurs on {111} planes and <110> directions, and dislocations typically have a ½<110> Burgers vector. The low defect density in the as-received material is characteristic of a material with a high potential to generate and store more defects during deformation. The observed

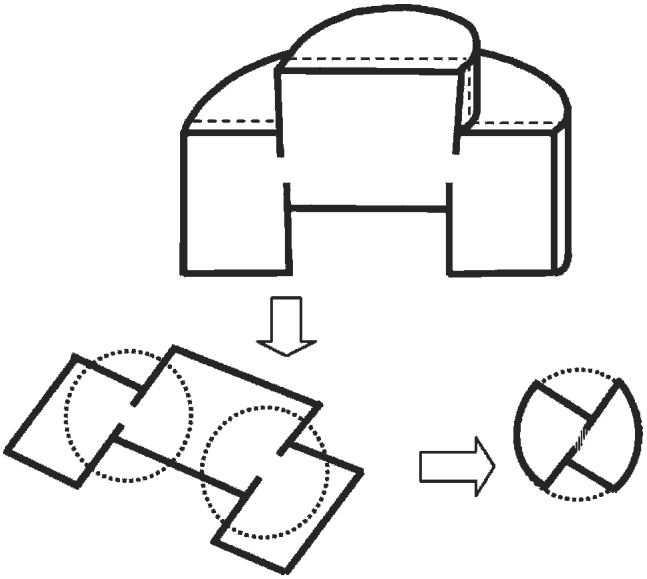

Fig. 1—TEM sample preparation of the hat-shaped specimen loaded in the dynamic forced shear configuration.

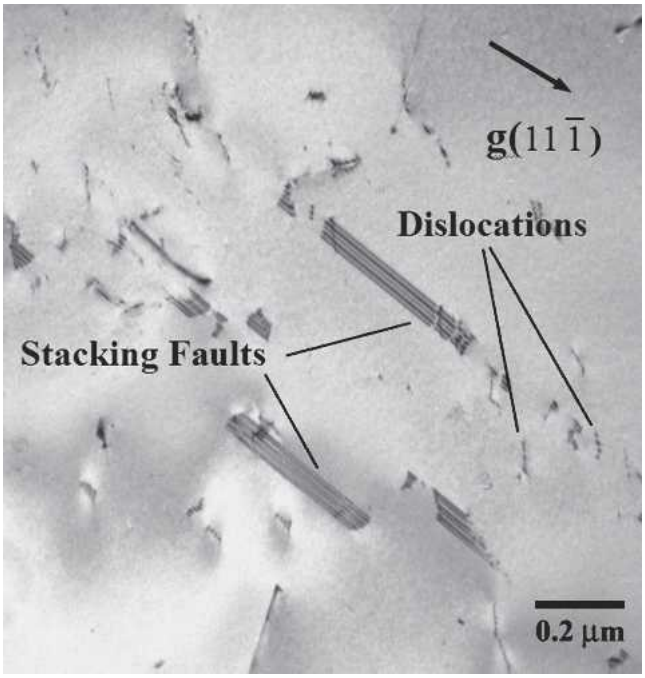

Fig. 2—Initial defects in the annealed 316L stainless steel; low density of dislocations and stacking faults scattered in a grain. The lower density of defects reflects the potentially higher capability for work hardening.

microstructure containing a low defect density is seen to correlate with its stable and linear hardening response during the first three stages of the forced shear tests for the annealed 316L SS (in Part I).

To correlate the TEM substructure to the microstructures observed optically, a brief review of the optically observed microstructural evolution, reported in Part I, is given here. The well-controlled forced shear tests on identical hat-shaped specimens were interrupted at six loading durations (25.1, 31.0, 36.1, 41.2, 51.5, and 61.8 μs, respectively) corresponding to different stages of shear localization. The optical metallography illustrated that the annealed 316L SS displayed a strong work-hardening effect and that localized deformation had not initiated until the sample was loaded to 41.2 μs. Just before the onset of shear banding, the sample loaded to 36.1 μs exhibited a heavily shear deformed section containing localized stream-like strips in the area close to the tips of the punch-in and punch-out ends. The center of the shear section was seen to display a heavy shear deformation but no localization. A full shear band did form in the sample loaded to 41.2 μs. Tiny fragments of grains with less deformed structure inside were observed to be scattered within the main shear band. A core region of the shear band was found to run through the entire shear section in the 51.5-μs sample. The shear band core with an average width of 10 μm is easily recognized by its sharp boundaries inside the shear band with a typical width of 60 μm. A well-developed shear band was observed in the sample loaded to 61.8 μs, and the shear band core was found to gradually grow to cover the entire shear band width.

The TEM examination performed in this current study concentrated on the evolving process of shear localization. The first two loading stages, during which work hardening dominated and no localized deformation occurred, are ignored in this study. The specimen loaded to 36.1 μs represents a critical stage just before the initiation of a shear band. The heavy shear deformation at this stage is seen to have generated a large number of defects: dislocation cell structures, bent deformation twin bands, and microbands. Figure 3 depicts the details of this heavily shear deformed region in which a large amount of dislocation cells and stretched grains exist. The selected area diffraction within these grains reveals a crystalline pattern (close to a (110) zone axis). The elongated diffraction spots along the circumferential direction imply that either the substructure contains some small-angle boundaries or the misorientations of significant magnitude in the local lattice exist. Stream-like strips with typical widths of 1~2 μm, reported in Part I, were seen to form in the area close to the tip of the punch-in end of the hat-shaped specimen and had some of the microstructural characteristics typically associated with shear localization. Figure 4(a) displays the substructure within such a stream-like strip embedded in a heavily shear deformed region. The marked strip exhibits a finer substructure than the outside regions. The ring diffraction pattern from the selected area, marked by a circle in the figure, indicates that multiple fine subgrains have been formed within this stream-like strip. The dimensions of these fine substructures are quite similar to those inside a shear band. Figure 4(b) shows a high-magnitude image of the substructure located at the upper-left portion of the circle in Figure

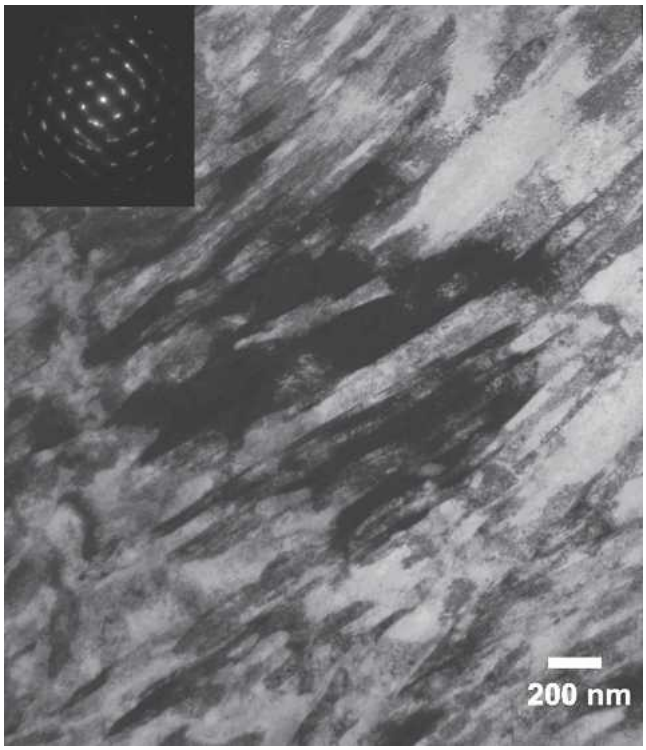

Fig. 3—Heavily sheared section on the hat-shaped specimen loaded before the initiation of shear localization.

4(a). It is obvious that these substructures came from the stretched dislocation cells. Before the initiation of shear localization, most of the previous equiaxed dislocation cells in these strips appeared to be stretched along the shear direction. The aspect ratio of these cells is larger than 4. The cell size is quite small, and a typical cell from the upper center of this image is about 300 nm in length and 60 nm in width. The high density of dislocation cells and the small dimensions characterize the formation process of these substructures. Since the perforation location of this TEM sample is close to the punch-in tip, the observed microstructure exposes more of the initial characteristics of the localized deformation. In fact, the middle part of the shear section of this sample still exhibits no localization but only heavy shear deformation. These observations exhibit what has occurred in the microstructure of 316L SS during the transition toward the onset of shear localization.

The sample loaded to 41.2 μs was seen to form a complete shear band in both the optical micrographs and the corresponding mechanical response. A micrographic montage of a partial shear band in Figure 5 clearly illustrates three distinct regions formed inside the shear band: an avalanched dislocation cell region, an elongated subgrain lath region, and a nearly rectangular or elliptical fine subgrain region. Close to the boundary of the shear band, a broad region covered by avalanched dislocation cells is observed and hence called the avalanched dislocation cell region. The original thick-walled dislocation cells are seen to be stretched out along the shear direction. Lateral dislocation walls along the shear direction were thinned due to the apparent annihilation of dislocations. New subgrain boundaries might have formed there. Meanwhile, at both

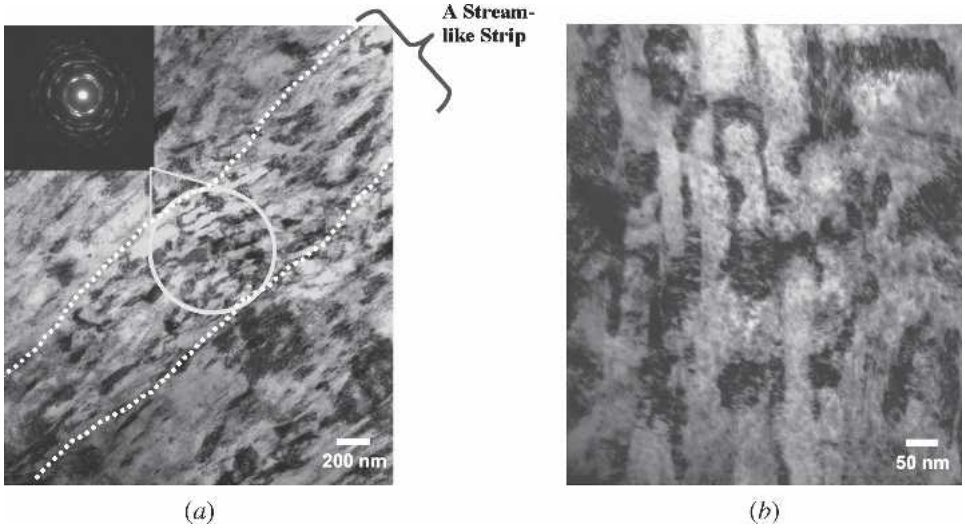

Fig. 4—(*a*) The steam-like strips display some fine substructure and the related selected area diffraction pattern shows some ring patterns. (*b*) The dislocation cells were stretched and elongated along the shear direction.

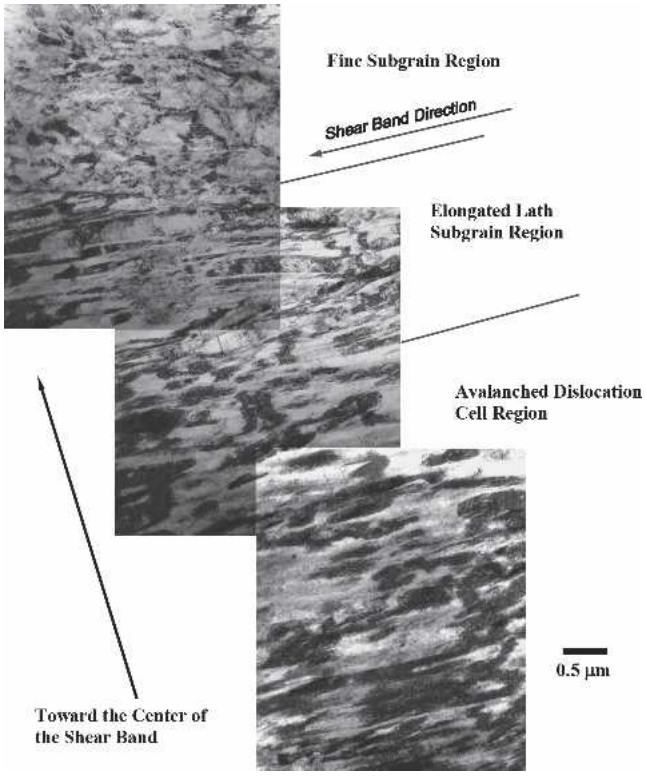

Fig. 5—Substructures within a shear band developed exactly at the onset of shear localization in the sample loaded to 41.2 μs exhibit three typical regions: an avalanched dislocation cell region, an elongated subgrain region, and a fine subgrain region. They sequentially appear from the shear band boundary toward the center of the shear band.

elongated ends of the cells, the dislocation walls have become thicker and thicker until the cells collapse (or tear up) into many black fragments containing high densities of tangled dislocations. This catastrophic collapse of the cells is therefore termed the avalanche of dislocation cells. Some disintegrated dislocation cells can still be traced to their original structures. In the avalanched dislocation cell region in Figure 5, the segments of avalanched dislocation cells exhibit fragments with (black) and without (bright) a high density of tangled dislocations. We refer to the individual domain of the fragments as a ''subcell.'' These subcells appear to have a substantially different contrast that reflects pronounced misorientations. Upon further deformation, they can create new boundaries with their neighbors and can form new subgrains. This process, in which the dislocation cells avalanche into fragments, build up new subcell boundaries, and thereafter lead to the formation of new subgrains, is characterized as a reconstruction of dislocation subcells and is one of the important mechanisms of the substructural refinement within shear bands.

Adjacent to the avalanched dislocation region is an elongated subgrain region. These subgrains were seen to be stretched along the shear direction in Figure 5. The narrow laths are rather long and have an extremely high aspect ratio (larger than 30). The formation of such laths seems to occur through a more complex mechanism than merely grain elongation. The 316L SS has 24 twin systems operative on {111} planes and <112> directions. Before the formation of shear bands, deformed grains were often observed to contain many deformation twins. A significant rotation near or inside a shear band inevitably led one or more twin systems to be activated and finally to reorient toward the shear band direction. These deformation twins rapidly multiplied until they reached a saturated state with a relatively narrow twin spacing. The multiplication of deformation twins is considered an important mechanism to generate the fine elongated laths arrayed along the shear direction. Grain elongation due to plastic flow alone could not have generated the same finely sized laths.

Across the elongated lath subgrain region toward the center of the shear band is the fine subgrain region. In the center of the shear band, nearly rectangular (or elliptical) subgrains are observed to replace the aligned lath subgrains. The fine subgrain structure is not uniform in morphology, and it is seen to be mixed with some stretched

laths. Figure 6(a) shows details of the mixed fine subgrain region where the elongated subgrains and the rectangular subgrains are coincident. Some fine equiaxed subgrains are also observed at the right side (circled area) in Figure 6(a). The average size of the fine subgrains is under 50 nm, and the number of such equiaxed subgrains in the shear band region under this loading duration is quite low.

Transition from the elongated substructure to the rectangular subgrains is the key to understand the grain refinement within shear bands. Figure 6(b) displays the details of such a transition among the mixed elongated and elliptical subgrains at the center of the shear band. Many of the fine subgrains appear to have been likely formed through a process of breaking down the elongated laths. An elongated lath of subgrain marked at A in Figure 6(b) was broken into two pieces that show the different contrast (the arrow marks the boundary). At the lateral side of subgrain A, a bamboo-shoot piece marked B was split from the parent subgrain A. This feature is likely the result of the lath subgrain interaction under shear stress. The splitting of subgrains is another important process thought to lead to subgrain refinement. A typical example is the long lath splitting shown on the left of Figure 6(b). The white lath subgrain (marked C) and the dark lath subgrain (marked D) likely belong to one parent lath. The shear deformation leads to the curved lath boundaries, and some portions appear to have been squeezed out to form a hump. The shear stress along the lath direction results in splitting lath C off from the long lath D. The bifurcation point E displays a clear bulge extruded toward the left of the figure (an arrow shows

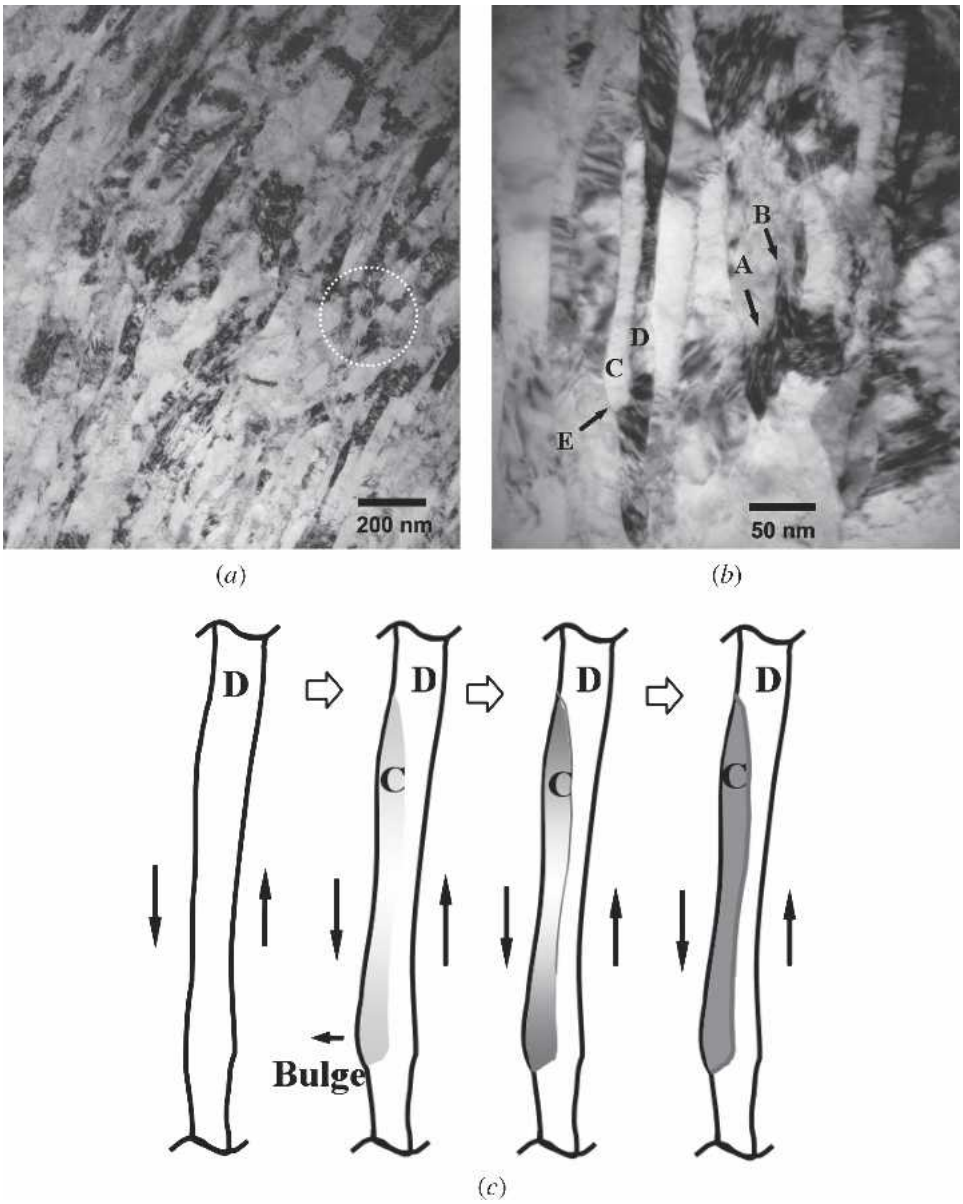

Fig. 6—(*a*) Alternate elongated subgrains and equiaxed fine subgrains at the center of the shear band at the onset of shear localization. (*b*) The stretched lath subgrains continue to be refined through the breakdown and the splitting. (*c*) A schematic splitting process of lath subgrain C from parent subgrain D shown in (*b*).

the extrusion direction) but retains a smooth boundary of the parent lath subgrain. A schematic drawing in Figure 6(c) depicts the complete process of the splitting of subgrain C from subgrain D. The split likely initiated from the upper portion and ended at the bifurcation point E. The heavy shear deformation and the softening of the lateral adjacent subgrains promote the formation of the extrusion and wavy boundaries. The shear force on these wavy interfaces leads to the uneven portions, which initiate a split and slide out. The above-mentioned evidence for grain refinement suggests that two mechanisms control the multiplication and the polygonization of the elongated subgrains: the breakdown and the splitting. The breakdown mechanism dominates the transverse segmentation of the elongated subgrains. The driving force comes from the conjugated shear stress. This mechanism primarily controls the transition from the elongated lath subgrains to the rectangular subgrains. The rectangular segments may slide out a little bit and generate new boundaries within their parent laths. The splitting mechanism represents an interaction between the adjacent elongated or rectangular subgrains. Once elongated laths develop some perturbations or humps, perhaps created through a transverse breakdown, their lateral boundaries become undulating. The adjacent subgrains push the humps to split apart from the parent laths. The split results in further narrowing of the elongated laths. The split portion at point E in Figure 6(b) has a width of only about 20 nm. This indicates that the elliptical or even equiaxed subgrains were developed under deformation-induced mechanisms, the breakdown and splitting, instead of from the nuclei of recrystallization. The temperature calculation in Part I of this paper indicates that the temperature rise within this shear band deformed under the 41.2-μs pulse is 470 °C (743K), which is lower than the recrystallization temperature of ~0.45 of the melting temperature (T_m = 1450 °C). Therefore, the development of subgrains may be completely controlled by a dynamic recovery.

The subsequent shear deformation was mainly localized into the shear band region once shear bands were initiated. The further development of shear localization in a sample loaded to 51.5 μs was observed to generate a core within the shear band. The optical micrographs of this sample reveal that the shear band core, formed within the 60-μm shear band, has a width of 10 μm. The corresponding TEM sample distinctly shows such a core area within the shear band and its unique characteristics. Figure 7 shows the substructure in the shear band core region with its extremely fine subgrains. There are three indications to support that the fine subgrain region is the shear band core. First, the dimension of the region is approximately 10 μm in width, consistent with the data observed in optical micrographs. Second, the extremely fine subgrains distinguish the core region from any substructure outside this region, even in the outer shear band. Third, all characteristics of the substructures outside the core, but within the shear band, are seen to be similar to what has been observed in the sample loaded to 41.2 μs.

The extremely fine substructure within the shear band core is shown in Figure 8(a). In contrast to the fine subgrain region in the 41.2-μs sample in Figures 6(a) and (b), the long lath subgrains completely disappear, and the combined equiaxed subgrains and elliptical subgrains filled the whole core region. In Figure 8(a), the fine subgrains are embedded in each other and are prone to form equiaxed shapes with curved boundaries. Unlike the initial stage of shear band formation shown in Figures 6(a) and (b), in which most of subgrains retained their long axis parallel to the shear direction, only scattered elliptical subgrains in Figure 8(a) expose the shear band direction to which their long axis is aligned. Equiaxed subgrains and curved subgrain boundaries have completely obliterated the trace of the shear deformation. Some equiaxed subgrains are easily seen to be broken apart from their parent elongated subgrains. Such types of linkages between the equiaxed subgrains and the elongated parent subgrains suggest that the equiaxed subgrains did not evolve from a process of nucleation and growth.

Figure 8(b) exhibits a close view of the fine subgrain region in the shear band core. Most of the subgrain boundaries

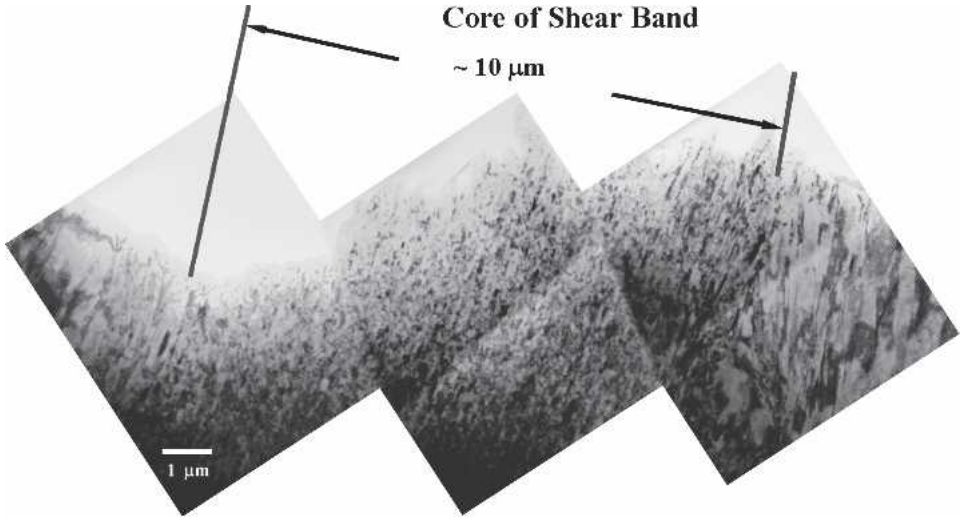

Fig. 7—A montage of the shear band core in the sample loaded to 51.5 μs. Extremely fine subgrains in the center of the image were observed within the core area, compared with other coarse stretched structures in the outer shear band.

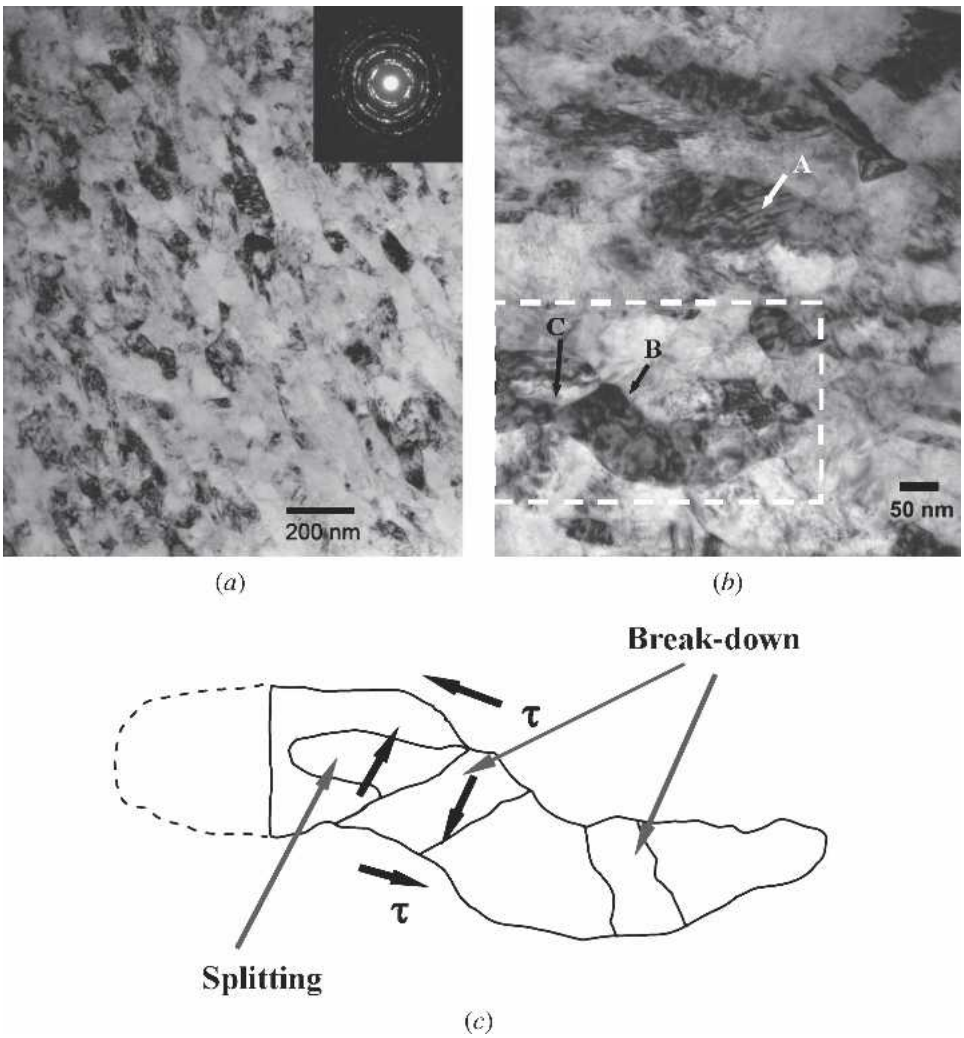

Fig. 8—(*a*) The extremely fine subgrains with an average grain size less than 100 nm in the shear band core region. (*b*) The coexistence of some equiaxed and ellipsoid subgrains that were broken down from the elongated subgrains, but with their long axes aligned along the shear band direction. (*c*) Schematic view of the breakdown and splitting processes in the area marked by the dashed lines in (*b*).

look blurred and have feather-like (fuzzy) patterns. The subgrain A contains a high density of defects and has been broken down into three sections; however, it still retains an overall rectangular shape. The lath marked by B in the figure appears to have been bent into a horizontal ''∼'' shape and was broken into several subgrains. The axis of the ''∼'' shape subgrain reveals the shear direction. Besides the obvious segmentation in the lath, a bamboo-shoot fine subgrain marked C in the figure appears split from the parent lath. Figure 8(c) shows a schematic view of the twisted parent lath. The transverse shear stress seems to have assisted in creating the broken pieces, and the sliding between the adjacent subgrains resulted in the generation of the split piece. Three characteristics are observed for the twisted lath: (1) the local temperature increase (up to 1207 °C estimated at this stage in Part I) led to the local thermal softening that allowed for a relative release of lateral confinement and made subgrain boundaries curved; (2) the lath experienced a large amount of rotation during lateral confinement release while it concurrently broke into several pieces of smaller subgrains; (3) both the breakdown and the splitting mechanisms dominate the refinement of the twisted subgrains. These patterns within the subgrains suggest that recrystallization was not the dominant mechanism to produce the refinement of the substructures, although the local temperature has been higher than the recrystallization criteria. If widespread recrystallization occurred, it could wipe out all of the initial deformed substructures. In addition, recrystallized products are frequently characterized as defect-free equiaxed subgrains. These features mentioned above have not been observed within the shear bands at this point in the evolving stage of shear band formation.

The further development of a shear band reflects the expansion of the shear band core during longer loading duration (61.8 μs). The shear band was almost entirely filled with shear deformation flow similar to that observed within the shear band core in the 51.5-μs sample. The montage in Figure 9 illustrates an area inside the shear band but close to a shear band boundary. The montage covers the transition area from the elongated lath subgrain region to the fine subgrain region that includes both the elliptical subgrains and the equiaxed subgrains. The elongated subgrains have

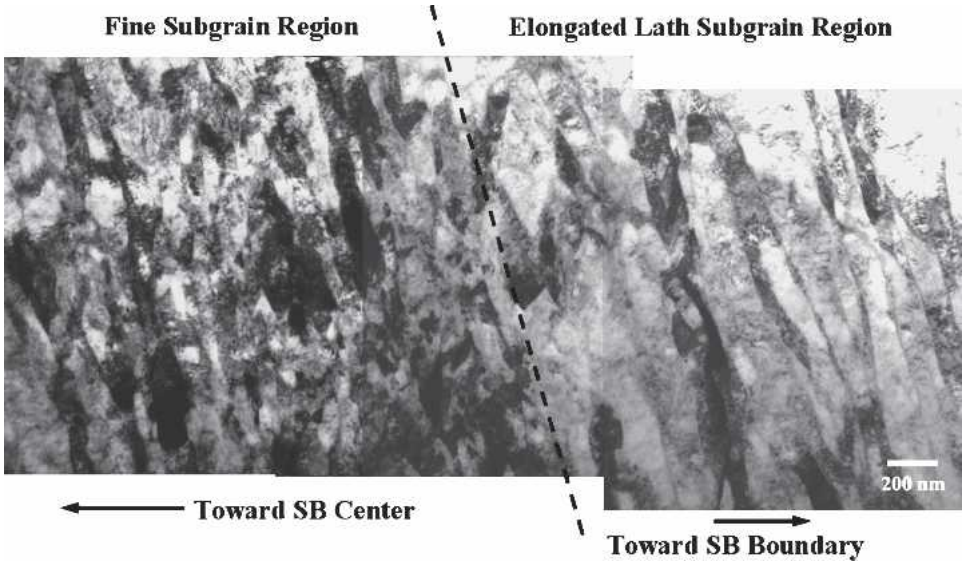

Fig. 9—A montage of the well-developed shear band in the 61.8-μs sample shows an area within the shear band but close to its boundary. The fine subgrain region and the elongated lath (subgrain) region are readily distinguished.

widths that range from 50~200 nm, and they are seen to be substantially wider than the long laths in Figure 6(a). This reflects the difference in the evolution of the substructures at the center of the band and at the boundaries. The appearance of the shear band core further softened the material at the shear band center, while the substructures at the shear band boundaries were thereafter subjected to relatively small shear deformation due to the unloading induced by the development of the core. The transition from the elongated laths to fine subgrains is abrupt and suggests that the fine subgrain region was expanding from the center of the shear band toward the band boundaries. In contrast, the coexistence of the equiaxed fine subgrains and elongated subgrains characterizes the process by which the heat flux corroded and engulfed the elongated lath subgrains. Except for a few long elongated subgrains, most of the reconstructed substructure consists of fine equiaxed subgrains where the shear flow direction is indistinct. When approaching the center of the shear band, the elongated subgrains disappear and only fine equiaxed subgrains remain at the center of the shear band. Figure 10 exhibits the details of the fine equiaxed subgrains in the shear band center where the shear flow direction is completely unrecognizable. These equiaxed subgrains possess a range of dimensions varying from 20 to 100 nm. Some small subgrains (~50 nm) with sharp grain boundaries are distributed randomly at the boundaries of larger subgrains. Such types of small subgrains may be the products of recrystallization.

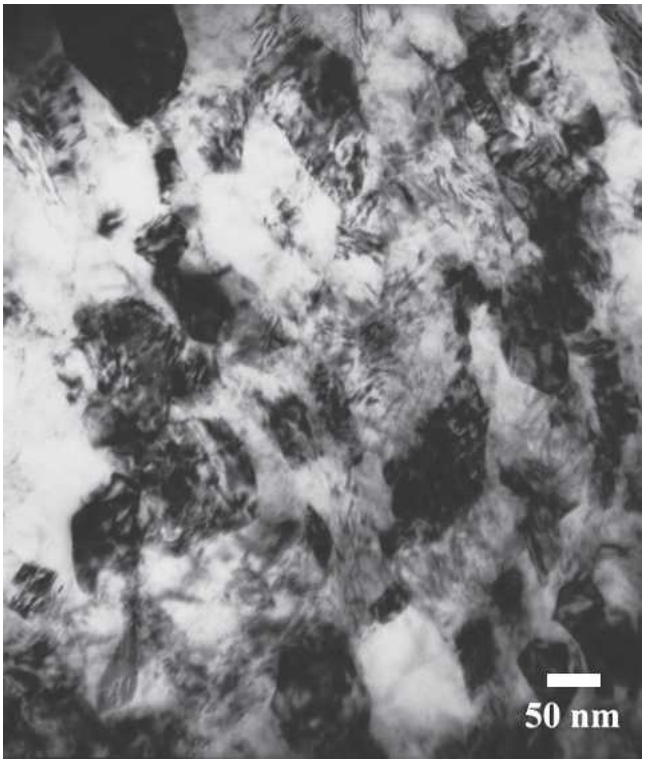

Fig. 10—Equiaxed subgrains appear at the center of the well-developed shear band. Some small subgrains with sharp boundaries exhibit features suggesting dynamic recrystallization.

IV. DISCUSSION

The adiabatic shear localization phenomenon was recognized in early investigations from the pronounced etching characteristics of the residual microstructure (white lines or white bands).[1,3] The white etching phenomenon in ferritic alloys, especially steels, was explained to be the result of a phase transformation. The early researchers[3] classified shear bands into two categories: deformed bands and transformation bands. The white etching bands represented a typical characteristic of phase-transformed bands in steels. In the current study, no white etching bands were observed.

The TEM analysis of the residual substructures within the shear bands indicates that no phase transformation occurred during the evolution of the shear band microstructures and no melting occurred. This latter conclusion is in agreement with the estimation of the temperature increment within the shear bands in Part I, where the maximum temperature rise was calculated to be 1408 °C, which is lower than the melting temperature of 316L SS (1450 °C). Of course, the temperature estimated in Part I of this paper depends on the measured maximum strain within the shear bands. Some micro- or nanoscale deformation, such as boundary sliding within shear bands, may lead to higher local strains and hence generated hot spots higher than the melting temperature. However, the microstructure resolved using TEM did not show any evidence to support the existence of melting.

Shear band studies within the past decade have indicated that some of the previously characterized transformation bands did not experience a true phase transformation. Some fine substructures found within these shear bands have been verified to be the products of dynamic recrystallization or dynamic recovery.[25–36] As summarized in the introduction, multiple mechanisms may individually operate or simultaneously coexist during shear localization according to the temperature and stress history experienced. The present TEM results cover a series of sequential stages after localization and illustrate several substructures, including avalanched dislocation cells, elongated lath subgrains, and equiaxed subgrains. The breakdown and splitting processes suggest that the grain refinement has been completed via a thermally assisted, shear deformation-induced mechanism instead of a thermally controlled phase transformation or growth of new grains. It is obvious that such a process lacks the nucleation/growth period and is not typical of the regular dynamic recrystallization process; rather, it may reflect some kind of deformation-induced grain refinement. Previous researchers have termed this process rotation recrystallization or continuous dynamic recrystallization.[37–40] Therefore, it is reasonable to believe that dynamic/static recovery controls the generation of subgrains with low-angle boundaries, and the continuous dynamic recrystallization may have assisted with the development of subgrains with high-angle boundaries through the breakdown and splitting of the substructure. Both dynamic recovery and dynamic recrystallization dominate the main development of substructure within shear bands in the present experiments. This is consistent with previous TEM analysis of shear bands in some other steels.[21,32] However, the well-developed shear bands loaded to 61.8 μs exhibited numerous equiaxed subgrains; some subgrains with sharp boundaries had some characteristics of regularly recrystallized grains. The proportion of such types of subgrains was quite low, and most of the subgrains in the same image had the apparent features of broken-down subgrains. The nucleation/growth type of dynamic recrystallization may occur at later stages during shear localization but does not appear to play a dominant role in the development of subgrains within shear bands due to the lack of sufficient time for widespread nucleation and growth as well as the quick quenching following the loading.

The substructures inside shear bands have been extensively studied in various materials, and some of the substructures observed in the present TEM examination have been reported previously in the literature. Highly elongated subgrains and equiaxed subgrains have been found within shear bands in various materials. Meyers *et al.*[30] studied shear localization in preshocked FCC copper using hat-shaped specimens and reported fine equiaxed subgrains with an average size of 50 nm inside the shear bands. Beatty *et al.*[31] applied a similar method to examine shear localization in AISI 4340 steel and observed that white etching bands formed. TEM examination of these bands revealed extremely fine equiaxed subgrains with a size range of 8~20 nm. They claimed that the extremely fine subgrains were heavily deformed martensite and no phase transformation occurred. Mgbokwere *et al.*[32] and Cho *et al.*[21] demonstrated that both highly elongated subgrains (laths) and fine equiaxed subgrains existed within shear bands in 4340 steel and in HY-100 steel, respectively. The breakdown process of the elongated substructure was also described in Reference 21. Xu *et al.*[22] announced that avalanched dislocation cells were observed within a shear band in a low-carbon steel. The appearance of avalanched dislocation cells symbolized the onset of shear localization. However, all these phenomena observed in the previous studies could not be associated with specific stages of shear banding at predefined locations. The current systematic investigation determined both the time and spatial locations for the appearance of these substructures within the time sequence of shear localization.

Stream-like strips appeared in the 316L SS sample just before the initiation of shear bands. They represent a characteristic of localized deformation at an early stage. The diffraction pattern indicates a ring structure that reflects the existence of fine subgrains in Figure 4(a). The appearance of stream-like strips is thought to be a foreshadowing of shear localization. Cho *et al.*[21] examined the less heavily deformed flank regions outside a shear band in HY-100 steel and found that the flow striations had a similar microstructure as that observed within shear bands. They postulated that the microstructure in the flow striations was representative of shear localization at an early stage. Their conjecture is substantiated by our observations. Conversely to their observations at the area adjacent to a shear band, the stream-like strips that we observed are exactly located on the path of a potential shear band before the formation of a full band.

The systematic TEM investigations of the main stages of shear localization provide more evidence to understand the mixed mechanisms under such a combined mechanical, physical, and metallurgical process. The coexistence of the three substructure regions inside a shear band is interpreted as the main characteristic of shear band onset in materials with a high work-hardening rate. Generally, the avalanched dislocation cells mainly exist in areas close to the shear band boundaries, while the fine subgrains are mainly present at the centers of shear bands where the maximum shear strain is operative. The elongated laths were frequently sandwiched between these two regions. The sizes of these three regions inside the shear bands shown in Figure 5 vary along the bands. They depend on not only the initial orientation of the grains before these grains involved into the localized deformation but also the deformation mode by which either the dislocation cell structures or the laminar

lath substructures predominated. However, the elongated laths do not appear to be the products of the avalanched dislocation cells. Not all shear band boundaries show an avalanched cell substructure. In some specific cases, only one mode appeared to connect with the fine subgrain region. Some shear band boundaries exhibited only elongated substructures. Although a quantification of the sizes of these regions is difficult, Figure 11 presents data representing the evolving process of a continuous expansion of the shear band core. The increasing width of the core and the decreasing size of the outer band substructure (combining the elongated lath and avalanched dislocation cell regions) are shown in this figure to shed light on how the shear band core evolves.

The evolution of the substructure inside the shear bands was observed to progress toward a fine equiaxed substructure. The TEM results show that there are two approaches for the evolution of shear band substructures: the subgrain reconstruction of the avalanched dislocation cells and the breakdown and splitting of elongated subgrains. Each is directly associated with the defect structure formed prior to the formation of shear localization. Figure 12 shows two schematic processes that characterize two different mechanisms controlling the refinement: the dislocation avalanche mechanism (Figures 12(a) through (d)) and the breakdown and splitting mechanism of the elongated subgrains (Figures 12(f) through (i)). The avalanche process requires the preexistence of dislocation cell structures before the formation of shear bands. The dislocation cells initially have a nearly equiaxed shape with thick dislocation walls (Figure 12(a)). Once these cells are deformed near a shear band, they are stretched and become elongated cells, as shown in Figure 12(b). Thick dislocation clusters are tangled and accumulated at both ends of the elongated cells, while dislocations annihilate at the lateral walls and form new subgrain boundaries (Figure 12(c)). Continued localized deformation tears up the dislocation cells and leads to the avalanched pattern that includes the fragments with high (black) and low (white) densities of tangled dislocations. These fragments were mentioned in the previous section as the dislocation subcells. Finally, these subcells generate new boundaries with their neighbors and individually construct new subgrains, as seen in Figure 12(d). The generation process of fine subgrains represents a reconstruction of dislocation subcells. The breakdown and splitting process evolves from the elongated lath substructures that result from either fine secondary twins or other elongated substructures, as shown in Figure 12(f). Figures 12(g) and (h) illustrate the breakdown and the splitting processes, respectively, although both processes may simultaneously happen. The breakdown reflects the transverse faults of the elongated subsubstructures that were locally sheared off to create rectangular subgrains, while the splitting reveals the longitudinal faults of the subgrains along the shear band direction to generate thinner laths. The shear stress provides the powerhouse for splitting along the shear direction (the longitudinal direction of elongated subgrains), while the conjugated shear stress becomes the main driving force to break down the elongated lath substructures into pieces in the transverse direction. At the later stage of shear banding, the elongated laths become curved due to adiabatic heating and provide more opportunities for the breakdown and splitting. The mixed breakdown and splitting leads to further refinement of subgrains, as seen in Figure 12(i). Localized deformation under these two mechanisms finally results in the generation of a very fine equiaxed subgrain structure, as shown in Figure 12(e). The development of this kind of substructure under either one of the two mechanisms can be attributed to a deformation-induced fragmentation process instead of a regular recrystallization process. The initial scales of the substructures in the two processes are quite different: the equiaxed dislocation cells are roughly a few microns in diameter, while the widths of the elongated laths are around 100~200 nm. Although the two processes generate different substructures at an early stage, further localized deformation brings them toward a similar pattern during late stages of localized deformation, at which time the multiple breakdown and splitting processes dominate the subsequent development of the substructures. This may involve deformation-induced or continuous dynamic recrystallization processes. Compared with the grain refinement afforded during severe plastic deformation (SPD),[41,42,43] such as equal channel angular pressing (ECAP) or high-pressure torsion (HPT), the microstructure within adiabatic shear bands is seen to be very similar to those after SPD. Although SPD is a deformation process in a quasi-static mode, severe shear and multiple paths built up a large shear deformation in local regions of the bulk materials. The accumulation process of defects and the subdivision of grains in both cases are the same; the only difference lies in the adiabatic heating in dynamic adiabatic shear bands, which may facilitate the development of localized deformation in their later stages.

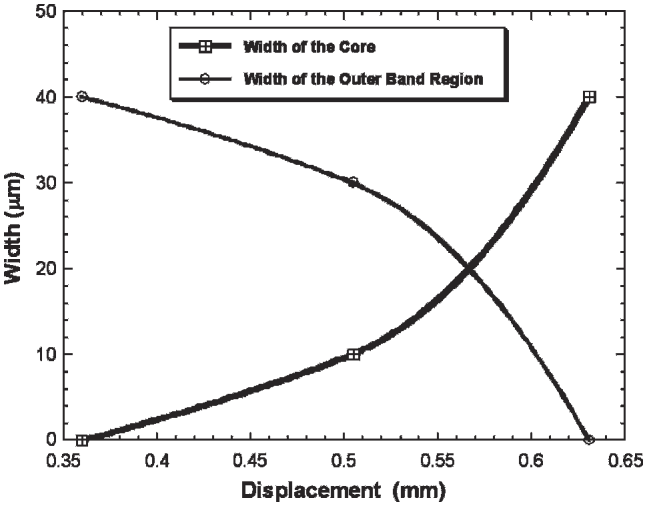

Fig. 11—The evolution of the shear band core width and the width of the outer band region as the function of increasing displacement. The shear localization initiated at a displacement of 0.36, and the final total displacement for a well-developed shear band is about 0.63.

The expansion of the shear band core was identified in Part I using OM. At the TEM observation level (10^2~10^3 higher than those observed in OM), a quantification of the dimensions of the substructural regions over a general view of fully developed shear bands is difficult due to the higher resolution and the perforation size limitation in the TEM.

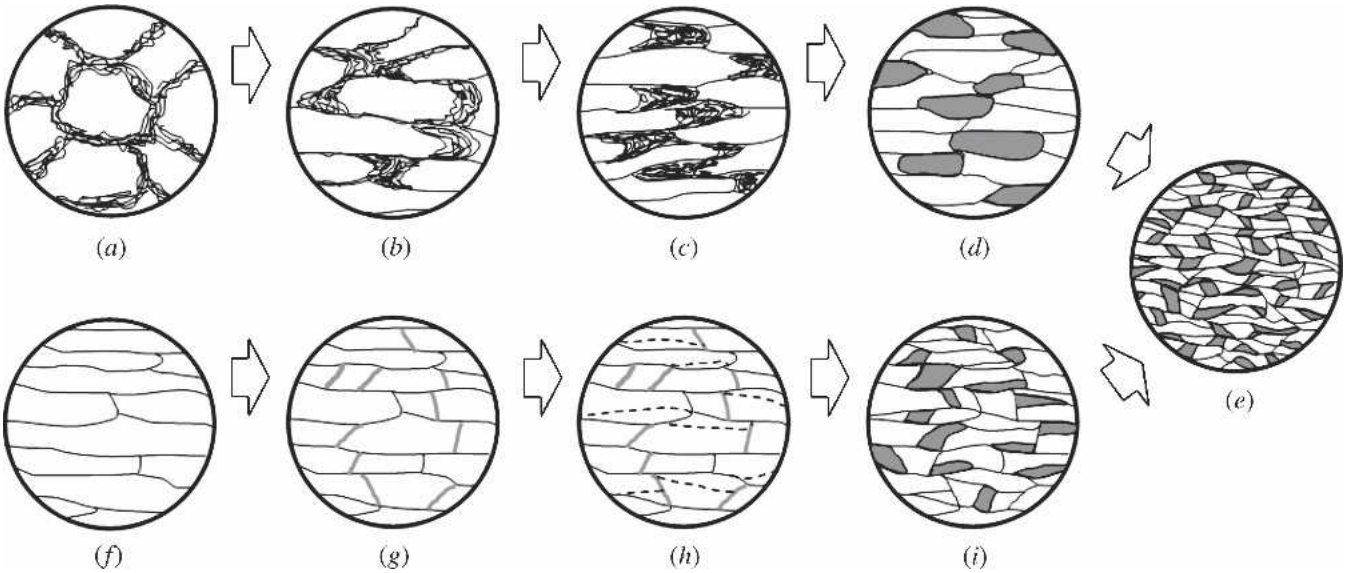

Fig. 12—Two main mechanisms for the refinement of substructures during shear localization: the dislocation avalanche mechanism (*a*) to (*d*) and the breakdown and splitting mechanism (*f*) to (*i*). The avalanche process evolves from (*a*) dislocation cell structures, (*b*) elongated cells, and (*c*) accumulated thick dislocation clusters and dislocation annihilation at lateral walls to (*d*) dislocation cell avalanche and the formation of elliptical subcells. The breakdown and splitting process evolves from (*f*) elongated laths (from secondary twins or other substructure), (*g*) broken-down rectangular pieces, and (*h*) splitting along the shear band to (*i*) the subgrain formation with curved boundaries during the combined breakdown and splitting processes. Both processes develop to the final fine equiaxed subgrain structure in (*e*).

However, some linkages between the observations in the OM and in the TEM can still be made. For instance, Figure 7 shows a montage of the core structure that is exactly matched with what was observed using the OM in Part I. The hardness in the 51.5-μs sample shows a pronounced jump in the shear band core region in Part I. The correlating TEM examination displays extremely fine subgrains within the shear band core. The fine subgrains should correspond to the highest hardness region. Although the core expanded to the whole shear band at a later stage (61.8-μs sample), the adiabatic heating generates a high temperature within the band and leads to dynamic recovery that slightly softens the material within the band. The measured hardness at this stage is more uniform within the band but is somewhat lower than that in the core region of the 51.5-μs sample.

Some recent studies have reported similar features inside shear bands in ultrafine grained and nanostructured metals,[44,45] though these shear bands were found to form under both quasi-static and dynamic loading conditions. These results are in good agreement with our observations of grain refinement within shear bands. The defect accumulation and the grain refinement, correlating to the macroscopic work hardening, appear to help trigger the formation of shear bands. Although the substructures within quasi-static shear bands in nanograined materials and within dynamic adiabatic shear bands in our coarse-grained material look similar, some differences are easily recognized. Because the nanograined materials start with a fine structure (100 to 200 nm), these grains during localized deformation evolved into an elongated laminar structure and break down to finer pieces. They do not require as extensive an accumulation of defects and subgrain formation. The adiabatic shear bands in coarse-grained materials require a significant increase in defect density, and high strain rate deformation therefore leads to the rapid tangling of dislocations to form subgrain boundaries. The ultra-fine-grained materials appear to bypass several stages for initiating a localized deformation, which is why the localized deformation can occur during the quasi-static loading without the help of adiabatic heating. The temperature within a shear band at an early stage of formation is not very high. This suggests that the increase of subgrain boundaries and the defect density will significantly constrain the conventional uniform plastic deformation and finally trigger a new, localized deformation mode. Although a high temperature was estimated within the later-stage shear band, evidence of an extensive recrystallization (discontinuous recrystallization) *via* nucleation and growth was not observed. The temperature there may be overestimated due to missing some nanoscale deformation mechanisms within shear bands, such as boundary sliding and subgrain rotation. Deformation under these mechanisms will not generate as much heat as calculated in the conventional work-heat transformation. If the discontinuous recrystallization fully occurred, it would eliminate all of the deformation-induced microstructure, such as the elongated subgrains. Therefore, although a few tiny dislocation-free subgrains appeared sporadically, dynamic recovery and continuous dynamic recrystallization are thought to dominate the shear localization.

V. CONCLUSIONS

The microstructural evolution of adiabatic shear localization in an annealed (as-received) 316L stainless steel was

systematically investigated using TEM. TEM examinations of adiabatic shear localization reveal a complete evolution of microstructure during shear localization. The major results are:

1. The substructures of shear bands at an early stage consist of three main regions: an avalanched dislocation cell region, an elongated lath subgrain region, and a fine subgrain region. Generally, the avalanched dislocation region appears close to the boundaries of the shear bands, while the fine subgrains exist close to the centers of the shear bands.
2. The shear band core initiated at a shear band center and comprised finer rectangular or elliptical subgrains and nearly equiaxed fine subgrains. These subgrains are clearly distinguished from the substructure in the outer shear bands.
3. The shear band core continuously expanded with an increase in displacement. The surrounding elongated subgrain regions are seen to be eroded by the spread of the fine subgrain region. The existence of elongated subgrains at the core boundaries implies that the localized deformation prefers to evolve into the core region. The outer shear band is finally eroded and annexed by the expansive core region.
4. The fine subgrains were seen to result either from the breakdown and splitting of elongated subgrains or from the reconstruction of subcells in the avalanched dislocation cell region. No evidence of melting was found within these bands during shear localization. Dynamic recovery and continuous dynamic recrystallization are considered the main mechanisms controlling the residual substructures within shear bands.

ACKNOWLEDGMENTS

This work was supported partly by the Joint Department of Defense (DoD) and Department of Energy (DOE) Munitions Technology Development Program. The authors thank Dr. Ellen Cerreta for her particularly helpful review of the manuscript and comments concerning the TEM analysis. Thoughtful discussions with Professors N. Thadhani, G. Ravichandran, and A.J. Rosakis are gratefully acknowledged. The assistance of Dr. C.M. Cady and Mr. M.F. Lopez is highly appreciated.

REFERENCES

1. H.C. Rogers: *Ann. Rev. Mater. Sci.*, 1979, vol. 9, pp. 283-311.
2. Y.L. Bai and B. Dodd: *Adiabatic Shear Localization, Occurrence, Theories and Applications*, Pergamon Press, Oxford, UK, 1992, p. 24.
3. M.E. Backman and S.A. Finnegan: in *Metallurgical Effects at High Strain Rates*, R.W. Rohde, B.M. Butcher, J.R. Holland, and C.H. Karnes, eds., Plenum Press, New York, NY, 1973, pp. 531-43.
4. R.F. Recht: *ASME(E) J. Appl. Mech. Trans.*, 1964, vol. 31, pp. 189-93.
5. R.J. Clifton: in *Material Response to Ultra-High Loading Rates*, NMAB-356, National Advisory Board (NRC), Washington, DC, 1980, Chapter 8.
6. T.W. Wright and J.W. Walter: *J. Mech. Phys. Solids*, 1987, vol. 35, pp. 701-20.
7. J.S. Costin, E.E. Crisman, R.H. Hawley, and J. Duffy: in *Proceedings of the Second Conference on the Mechanical Properties of Materials at High Rates of Strain*, Inst. Phys. Conf. Ser. No. 47, Oxford, 1979, pp. 90-100.
8. K.A. Hartley, J. Duffy, and R.H. Hawley: *J. Mech. Phys. Solids*, 1987, vol. 35, pp. 283-301.
9. A. Marchand and J. Duffy: *J. Mech. Phys. Solids*, 1988, vol. 36, pp. 251-83.
10. Y.L. Bai, Q. Xue, Y.B. Xu, and L.T. Shen: *Mech. Mater.*, 1994, vol. 17, pp. 155-64.
11. M. Zhou, A.J. Rosakis, and G. Ravichandran: *J. Mech. Phys. Solids*, 1996, vol. 44, pp. 981-1006.
12. J.J. Mason, A.J. Rosakis, and G. Ravichandran: *J. Mech. Phys. Solids*, 1994, vol. 42, pp. 1679-97.
13. H.C. Rogers and C.V. Shastry: in *Shock Waves and High Strain Rate Phenomena in Metals*, M.A. Meyers and L.E. Murr, eds., Plenum Press, New York, NY, 1981, pp. 285-98.
14. R.E. Winter: *Philos. Mag.*, 1975, vol. 31, pp. 765-73.
15. M.A. Meyers, G. Subhash, B.K. Kad, and L. Prasad: *Mech. Mater.*, 1994, vol. 17, pp. 175-93.
16. M.A. Meyers, Y.B. Xu, Q. Xue, M.T. Perez-Prado, and T.R. McNelley: *Acta Mater.*, 2003, vol. 51, pp. 1307-25.
17. J.V. Craig and T.A.C. Stock: *J Aust. Inst. Metals*, 1970, vol. 15, pp. 1-5.
18. T.A.C. Stock and K.R.L. Thompson: *Metall. Trans.*, 1970, vol. 1, pp. 219-24.
19. A.L. Wingrove: *J Aust. Inst. Metals*, 1971, vol. 16, pp. 67-70.
20. R.C. Glenn and W.C. Leslie: *Metall. Trans.*, 1971, vol. 2, pp. 2945-47.
21. K. Cho, S. Lee, S.R. Nutt, and J. Duffy: *Acta Metall. Mater.*, 1993, vol. 41, pp. 923-32.
22. Y.B. Xu, Y.L. Bai, Q. Xue, and L.T. Shen: *Acta Mater.*, 1996, vol. 44, pp. 1917-26.
23. Y. Me-Bar and D. Shechtman: *Mater. Sci. Eng.*, 1983, vol. 58, pp. 181-88.
24. H.A. Grebe, H.-R. Pak, and M.A. Meyers: *Metall. Trans.*, 1985, vol. 16A, pp. 761-75.
25. M.A. Meyers and H.-R. Pak: *Acta Metall.*, 1986, vol. 34, pp. 2493-99.
26. K.H. Hartman, H.D. Kunze, and L.W. Meyer: in *Shock Waves and High-Strain-Rate Phenomena in Metals*, M.A. Meyers and L.E. Murr, eds., Plenum Press, New York, NY, 1981, pp. 325-37.
27. C. Zener and J.H. Hollomon: *J. Appl. Mech.*, 1944, vol. 15, pp. 22-32.
28. M.C. Mataya, M.J. Carr, and G. Krauss: *Metall. Trans.*, 1982, vol. 13A, pp. 1263-74.
29. U. Andrade, M.A. Meyers, K.S. Vecchio, and A.H. Chokshi: *Acta Metall. Mater.*, 1994, vol. 42, pp. 3183-95.
30. M.A. Meyers, L.W. Meyer, J. Beatty, U. Andrade, K.S. Vecchio, and A.H. Chokshi: in *Shock Waves and High-Strain-Rate Phenomena in Materials*, M.A. Meyers, L.E. Murr, and K.P. Staudhammer, eds., Marcel Dekker, Inc., New York, NY, 1992, p. 529.
31. J.H. Beatty, L.W. Meyer, M.A. Meyers, and S. Nemat-Nasser: in *Shock Waves and High-Strain-Rate Phenomena in Materials*, M.A. Meyers, L.E. Murr, and K.P. Staudhammer, eds., Marcel Dekker, Inc., New York, NY, 1992, p. 645.
32. C.O. Mgbokwere, S.R. Nutt, and J. Duffy: *Mech. Mater.*, 1994, vol. 17, pp. 97-110.
33. K.A. Hartley, J. Duffy, and R.H. Hawley: *J. Mech. Phys. Solids*, 1987, vol. 35, pp. 283-301.
34. A. Marchand and J. Duffy: *J. Mech. Phys. Solids*, 1988, vol. 36, pp. 251-83.
35. J. Duffy and Y.C. Chi: *Mater. Sci. Eng.*, 1992, vol. A157, pp. 195-210.
36. A. Marchand, K. Cho, and J. Duffy: *The Formation of Adiabatic Shear Bands in an A1S1 1018 Cold-Rolled Steel*, Brown University Technical Report, October 1988.
37. M.A. Meyers, D.J. Benson, O. Vöhringer, B.K. Kad, Q. Xue, and H.-H. Fu: *Mater. Sci. Eng.*, 2002, vol. A322, pp. 194-216.
38. B. Derby: *Acta Metall.*, 1991, vol. 39, pp. 955-62.
39. J. Wang, Z. Horita, M. Furukawa, M. Nemoto, N. Tsenev, R. Valiev, Y. Ma, and T.G. Langdon: *J. Mater. Res.*, 1993, vol. 8, pp. 2810-18.
40. F.J. Humphreys and M. Hatherly: *Recrystallization and Related Annealing Phenomena*, Pergamon, Oxford, U.K., 2002, pp. 127-72
41. R.Z. Valiev, R.K. Islamgaliev, and I.V. Alexandrov: *Prog. Mater. Sci.*, 2000, vol. 45, pp. 103-89.
42. Y.T. Zhu and T.C. Lowe: *Mater. Sci. Eng.*, 2000, vol. A291, pp. 46-53.
43. Y.T. Zhu, J.Y. Huang, J. Gubicza, T. Ungár, Y.M. Wang, E. Ma, and R.Z. Valiev: *J. Mater. Res.*, 2003, vol. 18, pp. 1908-17.
44. Q. Wei, D. Jia, K.T. Ramesh, and E. Ma: *Appl. Phys. Lett.*, 2002, vol. 81, pp. 1240-42.
45. D. Jia, K.T. Ramesh, and E. Ma: *Acta Mater.*, 2003, vol. 51, pp. 3495-509.